NASA TN D-1423

TECHNICAL NOTE

D-1423

PREDICTED GAS PROPERTIES IN THE SHOCK LAYER AHEAD OF CAPSULE-TYPE VEHICLES AT ANGLES OF ATTACK

By George E. Kaattari

Ames Research Center
Moffett Field, Calif.

NATIONAL AERONAUTICS AND SPACE ADMINISTRATION
WASHINGTON

October 1962

NATIONAL AERONAUTICS AND SPACE ADMINISTRATION

TECHNICAL NOTE D-1423

PREDICTED GAS PROPERTIES IN THE SHOCK LAYER AHEAD OF CAPSULE-TYPE VEHICLES AT ANGLES OF ATTACK

By George E. Kaattari

SUMMARY

A method for determining shock-wave shapes, stagnation-point location, and flow-field properties for spherically blunt bodies at angle of attack was developed. The method is applicable to perfect gas flows and equilibrium flow of real gases. The results given by the method for shock surface and stagnation-point location are compared with experimental values. Comparison of the shock-layer density and temperature distribution are also made between the results of the method and those of a more exact procedure for a sphere. These comparisons indicate satisfactory agreement.

INTRODUCTION

During atmosphere entry, a vehicle is exposed to aerodynamic pressures and temperatures which are related to the strength and orientation of the detached shock about the forward portion of the vehicle. Present methods for predicting such shocks and the associated pressure, density, and temperature field (e.g., refs. 1 to 3) are generally limited to axisymmetric flow. Little attention has been given to the case of blunt bodies at angle of attack.

The purpose of this paper is to present a method for determining shock-wave shapes, stagnation-point location, and flow-field properties for blunt bodies at angle of attack. The method is an extension of reference 4 which treated shock-wave traces in the plane of symmetry. The present paper repeats these results with minor modifications and, in addition, considers shock traces in planes other than the plane of symmetry. The method presented is applicable to perfect gas flows and equilibrium flow of real gases. The first condition can occur at low Mach number ($M<7$) in air and the latter condition is approached at high Mach numbers when the recombination rate behind the shock is sufficiently rapid that equilibrium flow is attained in a distance that is small with respect to the shock-layer thickness.

NOTATION

B	angle between streamline on body and the geodesic drawn between a specified sonic point and the stagnation point, deg
f	shock correlation function of reference 4
h	distance from upper sonic point to stagnation point in plane normal to vehicle axis, ft
M	free-stream Mach number
P	pressure, lb/ft
q	normalized mass-flow gradient, $\frac{d(\rho_b V_b / \rho_b{}^* V^*_b)}{d(s/s^*)}$
R	radius, ft
r	radial coordinate with respect to vehicle axis of symmetry, ft
s	distance along body surface, ft
T	temperature, $^\circ R$
V	stream velocity, ft/sec
X,Y,Z	Cartesian coordinates
α	angle of attack, deg
β	angle between streamline and the φ plane at the shock wave, deg
γ	specific heat ratio
Δ	streamwise shock stand-off distance from point on body, ft
Δ_o	shock standoff distance on X-axis, ft
ϵ	half-angle subtended by capsule forebody arc, deg
ϵ_o	angle between the X-axis and the line drawn from the center of the forebody arc to the intersection of the forebody arc with the X-axis, deg
ϵ_{st}	angle between the line drawn from the stagnation point to center of forebody arc and the X-axis, deg
θ	slope with respect to free-stream direction, deg
ρ	density, slugs/ft^3

Φ angle between the plane containing the sonic point and the vehicle axis and the vertical plane of symmetry, deg

φ angular coordinate centered on X-axis with respect to vertical plane of symmetry, deg

φ' angle in plane normal to vehicle axis of symmetry measured between vertical plane and line containing a specified sonic point and the stagnation point on the vehicle face, deg

Subscripts

1 conditions just upstream of shock

2 conditions just downstream of shock

b body surface

s shock wave

st stagnation point

Superscripts

β β plane

l lower ($\varphi = 180^{\circ}$)

u upper ($\varphi = 0^{\circ}$)

* sonic point on body

ANALYSIS

In this section a method will be presented for defining the shock layer and gas-flow properties in front of a blunt vehicle at angle of attack such as shown in figure 1. The method is restricted to that portion of the shock layer in which the flow on the body surface is subsonic and to the angle-of-attack range $0<\alpha<\epsilon$ (fig. 2).

First the essential procedures of reference 4 for determining the shock trace in the vertical plane of symmetry are reviewed. The analysis is then extended to determine shock traces in other planes and thus to

define the shock surface. Methods for determining the gas properties immediately behind the shock surface, on the body surface, and within the shock layer between the shock and body surface follow in order.

Shock Surface

The shock surface will be defined as a system of circular-arc elements tangent to the Y-Z plane at the origin of the coordinate system X-Y-Z as shown in figure 2. The radius of these circular elements and the location of the body may be determined through application of continuity of mass flow between shock wave and body surface, oblique- and normal-shock-wave relationships, and the unique correlation between stagnation-point velocity gradient with Mach number for different bodies (ref. 5). In reference 4, particular application of the foregoing was made to develop a method for determining shock traces in the vertical plane of symmetry of blunt capsule vehicles at angle of attack. Essential equations and charts for this purpose are first reviewed and refined herein. Next, additional equations for the purpose of defining shock traces in other planes are developed, thus allowing the shock surface to be specified.

Shock trace in vertical plane of symmetry.- The shock-wave trace is composed of circular arc elements whose radii depend on the inclination and location of the sonic points on the body. The sonic-point inclination angles are functions of angle of attack α and the angle

$$\epsilon = \sin^{-1}(r_b/R_b) \tag{1}$$

The upper sonic point is usually located on the corner of the body and its inclination is

$$\theta_b^{*u} = 90^\circ - (\epsilon - \alpha) \tag{2a}$$

The lower sonic-point inclination θ_b^{*l} is given by a limiting angle $\theta^*_{b_{min}}$, corresponding to that for a sphere as determined from reference 1, if the lower corner inclination

$$\theta_b^l = 90^\circ - (\epsilon + \alpha) \tag{2b}$$

is less than $\theta^*_{b_{min}}$. If θ_b^l is greater than $\theta^*_{b_{min}}$, the lower sonic point is at the lower corner and thus $\theta_b^{*l} = \theta_b^l$ and is given by equation (2b). The values of θ_b^{*u} and θ_b^{*l} together with the appropriate normal shock-density ratio for the flight conditions involved prescribe the values of $(\Delta^*/R_s)^u$, θ_s^{*u}, and $(\Delta^*/R_s)^l$, θ_s^{*l}. These values, obtained from the charts of figure 3,[1] and the value of ϵ from equation (1) are used to calculate the vehicle sonic-point coordinates and shock radii, thus

[1]Figure 3 is a cross plot of figure 4 in reference 4 with appropriate changes in nomenclature.

locating the vehicle with respect to the shock trace. The necessary equations are

$$\frac{X^{*u}}{R_b} = \frac{(\cos\theta_b^{*u}+\cos\theta_b^{*l}) - (\sin\theta_b^{*u}-\sin\theta_b^{*l})\dfrac{\cos\theta_s^{*l}}{(\Delta^*/R_s)^l + (1-\sin\theta_s^*)^l}}{\dfrac{\cos\theta_s^{*u}}{(\Delta^*/R_s)^u + (1-\sin\theta_s^*)^u} + \dfrac{\cos\theta_s^{*l}}{(\Delta^*/R_s)^l + (1-\sin\theta_s^*)^l}} \quad (3)$$

$$\frac{Y^{*u}}{R_b} = \frac{X^{*u}}{R_b}\left[\frac{\cos\theta_s^{*u}}{(\Delta^*/R_s)^u + (1-\sin\theta_s^*)^u}\right] \quad (4)$$

$$\frac{R_s^u}{r_b} = \frac{Y^{*u}/R_b}{\sin\epsilon\cos\theta_s^{*u}} \quad (5)$$

and

$$\frac{R_s^l}{r_b} = \frac{\cos\theta_b^{*u} + \cos\theta_b^{*l} - (Y^{*u}/R_b)}{\sin\epsilon\cos\theta_s^{*l}} \quad (6)$$

In the above equations and in figure 3, changes from the nomenclature of reference 4 have been made and the shock and sonic-point inclinations are defined by the complementary angles of those previously used. The use of $\theta^*_{b_{min}}$ is a refinement to the procedure of reference 4 wherein $\theta^*_{b_{min}}$ of approximately 45° was used at all shock-density ratios. Two additional geometric properties associated with the shock trace in the vertical plane of symmetry are the shock standoff distance Δ_o and the location of the stagnation point shown in sketch (a). Calculation of these quantities is based on the simple assumptions that the stagnation streamline is perpendicular both to the normal portion of the shock (Y-axis at the origin) and to the body surface and that the curvature of the stream between the shock and the stagnation point is constant. For the standoff distance these considerations give

$$\frac{\Delta_o}{R_b} = \frac{X^{*u}}{R_b} + \cos(\epsilon - \alpha) - \cos\epsilon_o \quad (7)$$

where

$$\epsilon_o = \sin^{-1}\left[\frac{Y^{*u}}{R_b} - \sin(\epsilon - \alpha)\right] \quad (8)$$

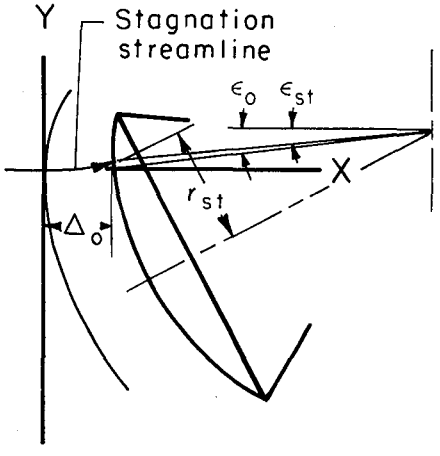

Sketch (a)

and for the stagnation-point location from the axis of symmetry

$$\frac{r_{st}}{r_b} = \frac{\sin(\alpha - \epsilon_{st})}{\sin \epsilon} \tag{9}$$

where

$$\epsilon_{st} \approx \sin^{-1}\left[\left(1 - \frac{\Delta_o}{2R_b}\right) \sin \epsilon_o\right] \tag{10}$$

The distance along the body from the stagnation point to the upper and lower sonic points is

$$\frac{s^{*u}}{r_b} = \frac{\epsilon - \alpha + \epsilon_{st}}{57.3 \sin \epsilon} \tag{11a}$$

and

$$\frac{s^{*l}}{r_b} = \frac{90^\circ - \theta_b^{*l} - \epsilon_{st}}{57.3 \sin \epsilon} \tag{11b}$$

Shock traces in other planes.- The analysis for shock traces other than in the plane of symmetry generally follows that for the plane of symmetry. Sketch (b) shows a φ plane containing the X-axis and rotated φ degrees with respect to the plane X-Y. The shock trace in this plane is curved and tangent at the origin to the Y-Z plane. To define the shock trace in question, it is first necessary to determine the sonic point standoff distance. For this purpose it is convenient to define the angle Φ between the plane containing the sonic point and the vehicle axis and the vertical plane of symmetry. The relationship between Φ and φ is

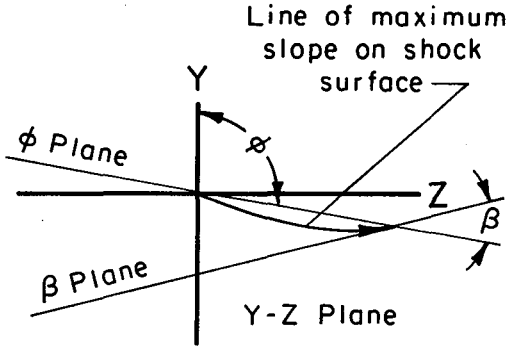

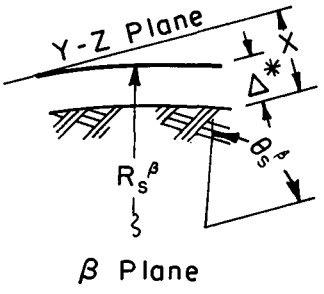

Sketch (b)

$$\varphi = \tan^{-1} \frac{\sin \Phi}{\frac{Y^{*u}}{r_b} - (1 - \cos \Phi) \cos \alpha} \tag{12}$$

The analysis of shock traces in the φ plane, unlike that for the vertical plane of symmetry, must generally account for deviations from radial flow. The direction of the maximum slope of the shock surface is represented by a curved line as

indicated in sketch (b). The flow directions immediately behind the shock follow this curved path and have the direction β with respect to the plane containing the sonic point and the X-axis. The sonic-point inclination on the body in the plane tangent to the departing flow and parallel to the X-axis (β plane) is assumed, as in reference 4, to determine uniquely the ratio of the sonic point standoff distance to the shock radius. The circular arc of this radius coincides tangentially with the Y-Z plane since it represents the projection on the β plane of a curved shock element proceeding from the origin.

The analysis is now reduced to a derivation of sonic point standoff distance from geometric considerations. Independent expressions for the X distance from the Y-Z plane to the sonic point, $R_s^{\beta}(1-\sin \theta_s^{*\beta}) + \Delta^*$ and $X^{*u} + r_b(1-\cos \Phi) \sin \alpha$, are equated and divided by the identity $R_s^{\beta} \cos \theta_s^{*\beta} = r_b \sin \Phi \cos \beta / \sin \varphi$, resulting in

$$\frac{(1-\sin \theta_s^*) + \Delta^*/R_s}{\cos \theta_s^*} = \frac{[X^{*u}/r_b + (1-\cos \Phi) \sin \alpha] \sin \varphi}{\sin \Phi \cos \beta} \tag{13}$$

Note that superscript β has been dropped and is to be understood in the following discussion. The left-hand term of equation (13) is a function of the shock-density ratio and an undetermined sonic-point inclination angle θ_b^*. The angles β and θ_b^* are also related by the equation

$$\cos \theta_b^* = \frac{\frac{\sin \epsilon \sin \Phi \cos \beta}{\sin \varphi} - \sin \epsilon_o \cos (\varphi-\beta)}{\cos\left\{\sin^{-1}\left[\frac{\sin \epsilon \sin \Phi \sin \beta}{\sin \varphi} + \sin \epsilon_o \sin (\varphi-\beta)\right]\right\}} \tag{14}$$

Since the left-hand terms of equations (13) and (14) are both functions of θ_b^*, the right-hand terms may be related. Figure 4 shows this relationship with shock-density ratio as the solid-line parameter. (The dashed line identified by the parameter q^* will be discussed in later sections.) The use of this chart is as follows: Coordinates for a curve with the abscissa calculated from equation (14) and the ordinate from equation (13) are found for three different choices of β. These coordinates are plotted in figure 4. The intersection of the curve defined by these coordinates with the appropriate shock-density ratio parameter locates $\cos \theta_b^*$ and, therefore, θ_b^*. With the value of θ_b^* known, Δ^*/R_s and θ_s^* can then be found from figure 3. The value of Δ^* of the shock-layer thickness at the sonic point located in the φ plane is

$$\frac{\Delta^*}{r_b} = \frac{(X^{*u}/r_b) + (1-\cos \Phi) \sin \alpha}{\frac{1 - \sin \theta_s^*}{\Delta^*/R_s} + 1} \tag{15}$$

A circular arc passing through this point and tangent to the Y-Z plane at the origin is then assumed to define the shock trace. This assumption implies that the distortion of the arc shape by projection from the φ plane to the β plane may be neglected.

It should be noted that for a portion of the lower part of the shock the flow is purely radial. The condition occurs at the φ plane in which the solution for $\cos \theta_b^*$ coincides on the curve $(\theta_{b_{min}}^*)$. Between this plane and $\varphi = 180^\circ$, the angle $\beta = 0^\circ$ and the shock radius has the constant value R_s^l given by equation (6).

Gas Properties at Shock Surface

The gas properties at the shock surface can be calculated if the free-stream properties are specified and the shock geometry is defined. To this end, each point on the shock surface is considered an element of a plane shock inclined at some angle with respect to the free-stream directions. This angle is that of the maximum inclination of the shock surface at the point in question. The shock-inclination angle θ_s^* opposite the sonic point in the β plane is determined as outlined in the previous section. The shock inclination along the circular shock arc from this point may be considered to increase linearly with arc length from θ_s^* to 90° at the origin. The flow properties behind the oblique shock are then determined with the equations of reference 6 for perfect gases or with the charts of references 7 and 8 for air in equilibrium flow or with similar charts that become available for other real gases.

In many cases the gas behind the shock will not be in equilibrium. A quantitative method leading to the estimation of the shock properties under these circumstances requires information on reaction rates of gases over a wider range of Mach numbers and densities than is currently available.

Gas Properties at Vehicle Surface

The analysis to be undertaken involves an infinitesimally thin streamtube on the vehicle surface. The flow process in the tube is considered an isentropic expansion from the previously calculated stagnation-point conditions. The pressure and other thermodynamic properties of the gas within the streamtube are calculated by an application of mass-flow continuity and isentropic flow relationships. Centrifugal effects are neglected and thus "one-dimensional" flow relationships are utilized.

The first step in the analysis is to determine the mass-flow $\rho_b V_b$ variation in a streamtube lying on the body surface. The surface is

considered divided into a series of streamlines radiating from the stagnation point. Two streamlines representing the projection of a streamtube on the vehicle surface are depicted in sketch (c). The width of the streamtube is assumed to increase linearly with distance from the stagnation point as if the flow were radial. Accordingly, the equation for continuity of radial mass flow given in reference 4 is utilized to evaluate the body surface mass flow $\rho_b V_b^*$ variation in the streamtube. This equation

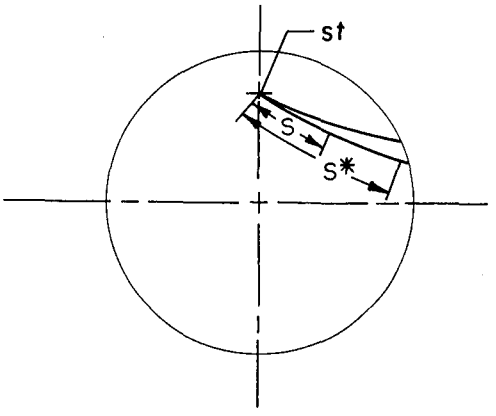

Sketch (c)

$$\frac{\Delta}{R_s} = \frac{\cos \theta_s}{\left(\frac{\rho_2}{\rho_1} - 1\right) \sin \theta_s \cos \theta_s + \left(\frac{\rho_b V_b}{\rho_1 V_1}\right) \sin \theta_b} \tag{16a}$$

is rearranged to give

$$\frac{\rho_b V_b}{(\rho_b V_b)^*} = \frac{\rho_1 V_1}{(\rho_b V_b)^*} \frac{\cos \theta_s}{\sin \theta_b} \left[\frac{1}{\Delta / R_s} - \left(\frac{\rho_2}{\rho_1} - 1\right) \sin \theta_s \right] \tag{16b}$$

The equation of shock-layer thickness

$$\frac{\Delta}{R_s} = \frac{\Delta_o}{R_s} + \frac{R_b}{R_s} (1 - \sin \theta_b) - (1 - \sin \theta_s) \tag{17}$$

and the relationship $R_b \cos \theta_b = R_s \cos \theta_s$ are combined and rearranged to give shock thickness Δ at θ_b (or θ_s) as a function of sonic-point shock-layer thickness Δ^* and sonic-point inclinations θ_b^* and θ_s^*:

$$\frac{\Delta}{R_s} = \frac{\Delta^*}{R_s} - \frac{\cos \theta_s^*}{\cos \theta_b^*} (\sin \theta_b - \sin \theta_b^*) - (\sin \theta_s^* - \sin \theta_s) \tag{18}$$

Equations (16b) and (18) can be combined to solve for the body mass-flow term $\rho_b V_b / (\rho_b V_b)^*$ as a function of θ_b or θ_s. With the additional relationship $s = R_b(\pi/2 - \theta_b)$, with θ_b measured in radians, for spherical surfaces or $s = R_s \cos \theta_s$ for a disc, it can be shown that equation (16b)

expands into an odd power series in s, the distance along the body surface

$$\rho_b V_b/(\rho_b V_b)^* = c_1(s/s^*) + c_3(s/s^*)^3 + \ldots$$

Two terms of this series give a simple and close approximation to equation (16b). The constants c_1 and c_3 are evaluated under the following conditions: (1) When $s = 0$, $\rho_b V_b = 0$ is automatically satisfied; (2) at $s = s^*$, $d[\rho_b V_b/(\rho_b V_b)^*]/d(s/s^*) = q^*$ is determined from the differentiation of (16b); and (3) at $s = s^*$, $\rho_b V_b/(\rho_b V_b)^* = 1$. A fourth condition applies when the flow passes through sonic values before reaching a corner: (4) then at $s = s^*$, $q^* = 0$. A function relating $\rho_b V_b$ to s consistent with the above enumerated boundary conditions is

$$\frac{\rho_b V_b}{(\rho_b V_b)^*} = \frac{3-q^*}{2}\left(\frac{s}{s^*}\right) + \frac{q^*-1}{2}\left(\frac{s}{s^*}\right)^3 \tag{19}$$

The final step in the analysis is to determine pressure as a function of length (s) along the streamtube. Since equation (19) gives the relationship between mass-flow ratio and distance along the body surface, the required pressure function can be found through mass-flow pressure relationships. For an ideal gas with constant γ the relationship is

$$\frac{\rho_b V_b}{(\rho_b V_b)^*} = \left(\frac{\gamma+1}{2}\right)^{\frac{1}{\gamma-1}} \sqrt{\frac{\gamma+1}{\gamma-1}} \sqrt{1 - \left(\frac{P}{P_{st}}\right)^{\frac{\gamma-1}{\gamma}}} \left(\frac{P}{P_{st}}\right)^{\frac{1}{\gamma}} \tag{20}$$

The values of pressure ratio as a function of s/s^* are found by combining equations (19) and (20) for various values of the index q^*. The results are presented in figure 5. Corresponding temperature and density functions may be calculated with the relationships

$$\frac{T}{T_{st}} = \left(\frac{P}{P_{st}}\right)^{\frac{\gamma-1}{\gamma}}$$

and

$$\frac{\rho}{\rho_{st}} = \left(\frac{P}{P_{st}}\right)^{\frac{1}{\gamma}}$$

For real gas in equilibrium flow, equation (19) is valid but the dependence between pressure and mass flow will generally require a step-by-step calculation. The index q^* is incorporated in the chart of figure 4 so that the appropriate pressure distribution along the streamline from the stagnation point to the sonic point is indicated simultaneously with the solution for θ_b^*. The pressure distribution may be assumed to lie on a straight line projected from the Y-Z plane on to the vehicle surface and extending from the stagnation point to the sonic point although the actual stream deviates from this projection as indicated in sketch (d). This

assumption introduces little error since the variation in pressure is relatively insensitive to small changes in path length. When the φ plane is on the vertical plane of symmetry ($\Phi = 0^{\circ}$), the angle θ_b^* is θ_b^{*u} (fig. 2), and the required q^* is located on figure 4 at the abscissa $\cos \theta_b^{*u}$ intersection with the appropriate density ratio ρ_2/ρ_1.

The actual path of a streamline on the vehicle surface can be determined approximately on the basis of an analysis presented in appendix B.

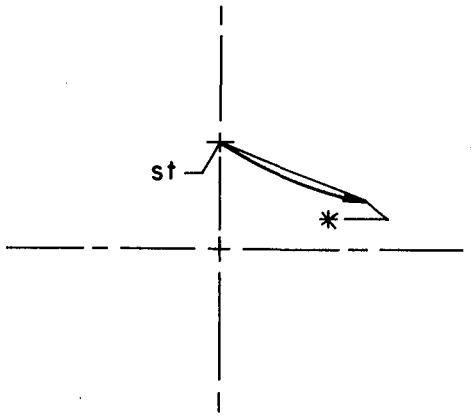

Sketch (d)

Temperature and Density Distribution in Shock Layer

The temperature and density in the shock layer are assumed to vary linearly from the shock to the vehicle surface. Since the value of temperature and density behind the shock and on the vehicle surface can be calculated as outlined in the previous sections, these properties within the shock layer are quickly determined. The results based on this simple structure are in fair accord with a more sophisticated theory for ideal gases as will be shown.

COMPARISONS OF ANALYTICAL AND EXPERIMENTAL RESULTS

The accuracy of the present method for predicting shock positions and gas properties in the shock layer is assessed by comparisons with the available results of experiment and with other theories. These comparisons are limited since no large body of experimental results exists, particularly in the range of high shock-density ratio where real gas effects occur.

This section of the report first compares the predicted and experimental shock envelope traces of a capsule vehicle in air at a Mach number of about 5.5 ($\rho_2/\rho_1 = 5.15$). Second, the results of the method in predicting temperature and density distribution in the shock layer of a sphere will be compared with the results of an exact theoretical method for a perfect gas. Third, a comparison of the predicted pressure distribution with Newtonian theory will be made for a capsule vehicle at different angles of attack. Finally, predicted stream patterns and stagnation-point locations on the forward face of a capsule vehicle at various angles of attack will be compared with experimental results.

Figure 6 shows experimental and predicted shock traces in various planes through a capsule vehicle for a shock-density ratio of about 5.15 and at various angles of attack. Good agreement is indicated between the experimental and predicted shock traces.

Figure 7 shows the estimated temperature and density variation in the forward shock layer about a sphere at two shock-density ratios for perfect gases. These values agree generally within 3 percent of those of the more exact results calculated with the methods of reference 2. At $\theta_b = 50^\circ$ the shock layer is at the boundary of the region to which the present method is restricted and agreement begins to deteriorate.

Figure 8 shows comparisons of the results of the method with Newtonian values for pressure distribution on a capsule vehicle at angle of attack. Newtonian theory is known to overestimate the pressure at "sonic corners." This is to be expected since Newtonian theory cannot anticipate and account for an expansion around a corner.

Figure 9 shows predicted and experimental stream patterns and stagnation-point locations. The results are for a Mach number of 3.3 ($\rho_2/\rho_1 = 4.11$) and angles of attack to 30°. The superposed solid lines on the photograph are predicted streamlines and are seen to be in fair accord with experiment, particularly at $\alpha = 20^\circ$. Good agreement between experimental and predicted stagnation-point locations is also indicated.

CONCLUDING REMARKS

A simple method of predicting shock envelopes about spherically blunt atmosphere entry vehicles at angle of attack was extended to include predictions of gas properties in the shock layer and on the forward surface of such vehicles. The method is applicable to perfect gas flows and to equilibrium flows of real gases. The results are presented in the form of charts for ease of computation.

Satisfactory agreement between predicted and experimental shock envelopes, vehicle surface streamlines, and stagnation-point locations was found for capsule vehicles in the Mach number range 3 to 6. Good agreement between the results of the present method and that of a more exact procedure for temperature and density variation in the shock layer of a sphere was found for two shock-density ratios.

Ames Research Center
National Aeronautics and Space Administration
Moffett Field, Calif., May 18, 1962

APPENDIX A

NUMERICAL EXAMPLES

The method is now applied to the prediction of the shock trace, the pressure on the body, and the temperature and density distribution of the shock layer in the φ plane containing the X-axis and the sonic point on the body at $\Phi = 60^\circ$. The vehicle has a face of ratio $r_b/R_b = 0.5$ subtending the angle $\epsilon = 30^\circ$ (eq. (1)). The angle of attack is $\alpha = 25^\circ$ and the Mach number is 5.

It is first necessary to evaluate equations (2) and (11) to establish the shock standoff distance and stagnation-point location which are common to shock traces in all planes. At Mach number 5, the normal shock-density ratio in ideal air is 5. The value of $\theta^*_{b_{min}}$ at this density ratio is determined from figure 3 as 49.2°. Equation (2) gives the upper sonic point inclination $\theta_b^{*u} = 90^\circ - (\epsilon-\alpha) = 85^\circ$ and the lower corner inclination $\theta_b^{l} = 90^\circ - (\epsilon+\alpha) = 35^\circ$. Since the latter angle is less than $\theta^*_{b_{min}} = 49.2^\circ$, the lower sonic point does not lie on the corner, but on the capsule face where $\theta_b^{*l} = 49.2^\circ = \theta^*_{b_{min}}$. With these angles and the parameter $\rho_2/\rho_1 = 5$, $(\Delta^*/R_s)^u = 0.103$, $\theta_s^{*u} = 75^\circ$, $(\Delta^*/R_s)^l = 0.171$, and $\theta_s^{*l} = 62.5^\circ$ are found from figure 3. The following equations may now be evaluated:

$$\frac{X^{*u}}{R_b} = \frac{(0.087 + 0.654) - (0.996 - 0.757)\dfrac{0.462}{0.171 + 0.113}}{\dfrac{0.259}{0.103 + 0.034} + \dfrac{0.462}{0.171 + 0.113}} = 0.100 \qquad (3)$$

$$\frac{Y^{*u}}{R_b} = 0.100 \times 1.890 = 0.189 \qquad (4)$$

$$\frac{R_s^u}{r_b} = \frac{0.189}{0.500 \times 0.259} = 1.46 \qquad (5)$$

$$\frac{R_s^l}{r_b} = \frac{0.087 + 0.654 - 0.189}{0.500 \times 0.462} = 2.40 \qquad (6)$$

$$\frac{\Delta_o}{R_b} = 0.100 + 0.996 - 0.995 = 0.101 \qquad (7)$$

$$\epsilon_o = \sin^{-1}(0.189 - 0.087) = 5.9^\circ \qquad (8)$$

$$\frac{r_{st}}{r_b} = \frac{\sin (25^\circ - 5.5^\circ)}{0.500} = 0.668 \tag{9}$$

$$\epsilon_{st} = \sin^{-1} [(1 - 0.050)\ 0.102] = 5.5^\circ \tag{10}$$

$$\frac{s^{*u}}{r_b} = \frac{30^\circ - 25^\circ + 5.5^\circ}{57.3^\circ \times 0.500} = 0.367 \tag{11a}$$

$$\frac{s^{*l}}{r_b} = \frac{90^\circ - 49.2^\circ - 5.5^\circ}{57.3^\circ \times 0.500} = 1.23 \tag{11b}$$

The above values define the shock trace in the vertical plane of symmetry and establish the stagnation-point location and shock standoff distance. We may now proceed to define the shock trace in the plane containing the sonic point at location $\Phi = 60^\circ$. Equation (12) gives

$$\varphi = \tan^{-1} \frac{0.866}{0.378 - 0.500 \times 0.906} = 95^\circ \tag{12}$$

The right-hand terms of equations (13) and (14) are evaluated

$$\frac{\left[\frac{x^{*u}}{r_b} + (1 - \cos \Phi) \sin \alpha\right] \sin \varphi}{\sin \Phi \cos \beta} = \frac{[0.200 + 0.500 \times 0.423]\ 0.995}{0.866 \cos \beta}$$

$$= \frac{0.472}{\cos \beta} \tag{13}$$

and

$$\frac{\frac{\sin \epsilon \sin \Phi \cos \beta}{\sin \varphi} - \sin \epsilon_o \cos (\varphi - \beta)}{\cos\left\{\sin^{-1}\left[\frac{\sin \epsilon \sin \Phi \sin \beta}{\sin \varphi} + \sin \epsilon_o \sin (\varphi - \beta)\right]\right\}}$$

$$= \frac{0.435 \cos \beta - 0.102 \cos (95^\circ - \beta)}{\cos\left\{\sin^{-1}\left[0.435 \sin \beta + 0.102 \sin (95^\circ - \beta)\right]\right\}} \tag{14}$$

Trial values of 0°, 15°, and 30° for β are used to make the tabulation

β, deg	Ordinate eq. (13)	Abscissa eq. (14)
0	0.472	0.446
15	.489	.412
30	.545	.351

and the values are plotted in figure 4 giving the indicated curve which intersects with the parameter $\rho_2/\rho_1 = 5$ at the abscissa $\cos \theta_b^* = 0.355$; thus $\theta_b^* = 69.2^\circ$. From figure 3, $\theta_s^* = 71.1^\circ$ and $(\Delta^*/R_s) = 0.121$. The shock stand-off distance in the φ plane at the sonic point is then evaluated with equation (15)

$$\frac{\Delta^*}{r_b} = \frac{0.200 + 0.500 \times 0.423}{(0.043/0.121) + 1} = 0.303 \qquad (15)$$

The shock surface trace in the φ plane is a circular arc drawn tangent to the Y-Z plane at the origin and passing through the point at distance Δ^* in the free-stream direction from the corner of the vehicle face at $\Phi = 60^\circ$. Along this arc the maximum shock surface inclination is assumed to vary linearly with arc length from $\theta_s^* = 71.1^\circ$ opposite the sonic-point to $\theta_s = 90^\circ$ at the origin. The conditions behind the shock trace are determined from the Rankine-Hugoniot relations for oblique shocks in ideal air at $M = 5$.

The pressure, density, and temperature distributions on the body in the φ plane are fixed by q^* which is determined simultaneously with $\cos \theta_b^*$ from figure 4. For this numerical example, $q^* \approx 1.0$ and $\gamma = 1.4$. The appropriate pressure ratios with respect to the stagnation-point values are selected from figure 5. Corresponding density and temperature ratios are computed from $\rho/\rho_{st} = (P/P_{st})^{1/\gamma}$ and $T/T_{st} = (P/P_{st})^{(\gamma-1)/\gamma}$.

The values of pressure, density, and temperature are now known on the shock and vehicle traces in the φ plane. The conditions in the shock layer between these bounds are estimated by linear interpolation.

APPENDIX B

BODY STREAMLINE CURVATURE

When the vehicle is at angle of attack, the streamlines on the capsule face will curve because of nonaxisymmetric pressure distribution. An analysis of this curve is made utilizing the well-known relationship

$$\frac{1}{R} = \frac{dP/dn}{\rho V^2} \tag{B1}$$

where $1/R$ is the stream curvature in a plane tangent to the vehicle face and n is a coordinate normal to the streamline in the same plane.

Evaluation of the pressure gradient in equation (B1) proceeds as follows: The body pressure as determined in previous analysis is a function of the variables s/s^* and q^*. The pressure function is found by combining equations (19) and (20)

$$\mathbf{P}\left(\frac{P}{P_{st}}\right) = \left(\frac{\gamma+1}{2}\right)^{\frac{1}{\gamma-1}} \sqrt{\frac{\gamma+1}{\gamma-1}} \sqrt{1 - \left(\frac{P}{P_{st}}\right)^{\frac{\gamma-1}{\gamma}}} \left(\frac{P}{P_{st}}\right)^{\frac{1}{\gamma}} = \frac{3 - q^*}{2} \frac{s}{s^*} + \frac{q^* - 1}{2} \left(\frac{s}{s^*}\right)^3$$

The total derivative on the pressure function $\mathbf{P}$ with respect to n is

$$\frac{d\mathbf{P}}{dn} = \frac{\partial \mathbf{P}}{\partial(s/s^*)} \frac{d(s/s^*)}{dn} + \frac{\partial \mathbf{P}}{\partial q^*} \frac{dq^*}{dn}$$

$$= -\left[\frac{3 - q^*}{2} + \frac{3(q^* - 1)}{2} \left(\frac{s}{s^*}\right)^2\right] \frac{s}{s^{*2}} \frac{ds^*}{dn} + \frac{1}{2}\left[\left(\frac{s}{s^*}\right)^3 - \left(\frac{s}{s^*}\right)\right] \frac{dq^*}{dn} \tag{B2}$$

where $\frac{d(s/s^*)}{dn} = \frac{1}{s^*} \frac{ds}{dn} - \frac{s}{s^{*2}} \frac{ds^*}{dn}$ and $\frac{ds}{dn} = 0$ (orthogonal coordinates).

In order to determine the derivative of q^*, its dependence on the flow path parameters must be known. It can be found, by differentiating equation (19) with respect to s/s^*, that the stagnation-point mass-flow derivative q_{st} given when $s/s^* = 0$ is $(3-q^*)/2$. It can also be determined from reference 4 that

$$q_{st} = (\rho_1 V_1 / \rho_b^* V_b^*)(1 + \Delta_o/R_b)(\rho_{st}/\rho_1)(f/2)(s^*/\Delta_o)$$

All terms in the foregoing expression are constant except in the case of angle of attack, the distances (s^*) to the sonic points vary. Therefore, $q_{st} = cs^*$, so $q^* = 3-2cs^*$. The derivative

$$dq^*/dn = (dq^*/ds^*)(ds^*/dn) = -(2q_{st}/s^*)(ds^*/dn)$$

so

$$dq^*/dn = [(q^* - 3)/s^*](ds^*/dn)$$

It remains to determine the derivative ds^*/dn required in (B2). The relationship of the differentials ds^* and dn is shown in figure 10. Two differentially displaced streamlines are depicted between which the pressure gradient is sought. The streamlines are assumed to diverge linearly with distance from the stagnation point. Due to this divergence the differentials $dn = sr_b\, d\Phi \cos \xi/s^*$ and $ds^* = -r_b\, d\Phi \sin \xi$ are obtained giving the derivative $ds^*/dn = -s^* \tan \xi/s$. Substituting these in equation (B2) gives the simple result

$$\frac{d\mathbf{P}}{dn} = q^* \left(\frac{s}{s^*}\right) \frac{\tan \xi}{s} \tag{B3}$$

The pressure function derivative $d\mathbf{P}/dn$ in terms of the required pressure derivative dP/dn is

$$\frac{d\mathbf{P}}{dn} = \frac{\left(\frac{\gamma+1}{2}\right)^{\frac{1}{\gamma-1}} \sqrt{\frac{\gamma+1}{\gamma-1}}}{\gamma} \left[\sqrt{1 - \left(\frac{P}{P_{st}}\right)^{\frac{\gamma-1}{\gamma}}} \left(\frac{P}{P_{st}}\right)^{\frac{1-\gamma}{\gamma}}\right] \left[1 - \frac{\frac{\gamma-1}{2}\left(\frac{P}{P_{st}}\right)^{\frac{\gamma-1}{\gamma}}}{1 - \left(\frac{P}{P_{st}}\right)^{\frac{\gamma-1}{\gamma}}}\right] \frac{dP}{P_{st}\, dn} \tag{B4}$$

The value of the pressure derivative is put in equation (B1) resulting in

$$\frac{\rho_b V_b^2}{R} = \frac{P\gamma \left(\frac{s}{s^*}\right)^3 \frac{\tan \xi}{s} q^*}{\frac{\rho_b V_b}{(\rho_b V_b)^*} \left[1 - \frac{\frac{\gamma-1}{2}\left(\frac{P}{P_{st}}\right)^{\frac{\gamma-1}{\gamma}}}{1 - \left(\frac{P}{P_{st}}\right)^{\frac{\gamma-1}{\gamma}}}\right]} \tag{B5}$$

When the pressure ratio is replaced by the computationally more convenient temperature ratio, the following expression results

$$\frac{1}{R} = \frac{\frac{\gamma - 1}{2} \frac{T}{T_{st}} q^* \left(\frac{s}{s^*}\right)^2 \frac{\tan \xi}{s}}{\left\{\left(\frac{3 - q^*}{2}\right)\left[1 - \left(\frac{s}{s^*}\right)^2\right] + \left(\frac{s}{s^*}\right)^2\right\}\left(1 - \frac{\gamma + 1}{2} \frac{T}{T_{st}}\right)} \tag{B6}$$

Graphical constructions of flow paths for various values of q^* were made by use of equation (B6) with $\gamma = 1.4$. The angles B_{st} and B^* with respect to the direction

$$\varphi' = \tan^{-1} \frac{\sin \Phi}{(h/r_b) - (1 - \cos \Phi)} \tag{B7}$$

where

$$h/r_b = 1 - \sin(\alpha - \epsilon_{st})/\sin \epsilon$$

were determined graphically from these constructions and are shown as functions of $\varphi' - \Phi$ for various values of q^* in figure 11. With the angles B determined, the flow path can be closely approximated by a curve of uniformly increasing curvature drawn tangent to the flow directions B_{st} and B^* as indicated in the lower portion of figure 10. It is felt that the effect of γ on the flow direction angles is not large and figure 11 may be used to approximate flow paths for gases of γ different from 1.4.

For the numerical example considered in appendix A, $(\varphi' - \Phi) = 100.8^\circ - 60^\circ = 40.8^\circ$ and $q^* = 1.0$. With these values, $B^* = 15^\circ$ and $B_{st} = 6^\circ$ are determined from figure 11.

REFERENCES

1. Van Dyke, Milton D., and Gordon, Helen D.: Supersonic Flow Past a Family of Blunt Axisymmetric Bodies. NASA TR R-1, 1959.

2. Fuller, Franklyn B.: Numerical Solutions for Supersonic Flow of an Ideal Gas Around Blunt Two-Dimensional Bodies. NASA TN D-791, 1961.

3. DeL'Estoile, H., and Rosenthal, L.: Rapid Evaluation of Radiant Heating During Re-entry into the Atmosphere. Aeronautics and Astronautics - Proceedings of the Durand Centennial Conference. August 1959, Pergamon Press, New York, 1960, pp. 173-203.

4. Kaattari, George E.: Predicted Shock Envelopes About Two Types of Vehicles at Large Angles of Attack. NASA TN D-860, 1961.

5. Traugott, Stephen C.: An Approximate Solution of the Direct Supersonic Blunt-Body Problem for Arbitrary Axisymmetric Shapes. Jour. Aero. Sci., vol. 27, no. 5, May 1960, pp. 361-370.

6. Ames Research Staff: Equations, Tables and Charts for Compressible Flow. NACA Rep. 1135, 1953.

7. Hochstim, Adolph R.: Gas Properties Behind Shocks at Hypersonic Velocities. I. Normal Shocks in Air. Convair Rep. ZPh(GP)-002, January 30, 1957.

8. Moeckel, W. E., and Weston, Kenneth C.: Composition and Thermodynamic Properties of Air in Chemical Equilibrium. NACA TN 4265, 1958.

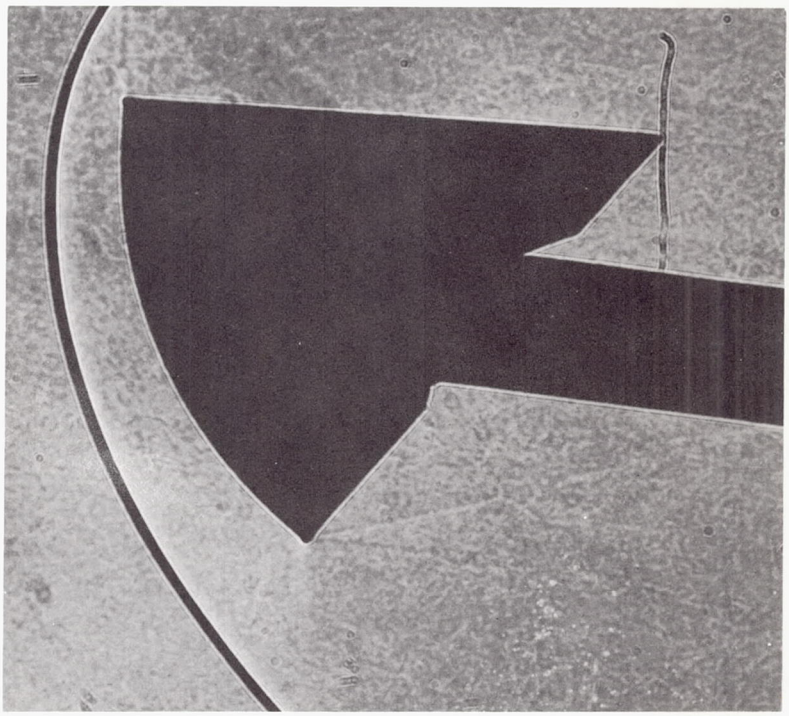

A-29291

Figure 1.- Shock wave due to blunt vehicle at angle of attack.

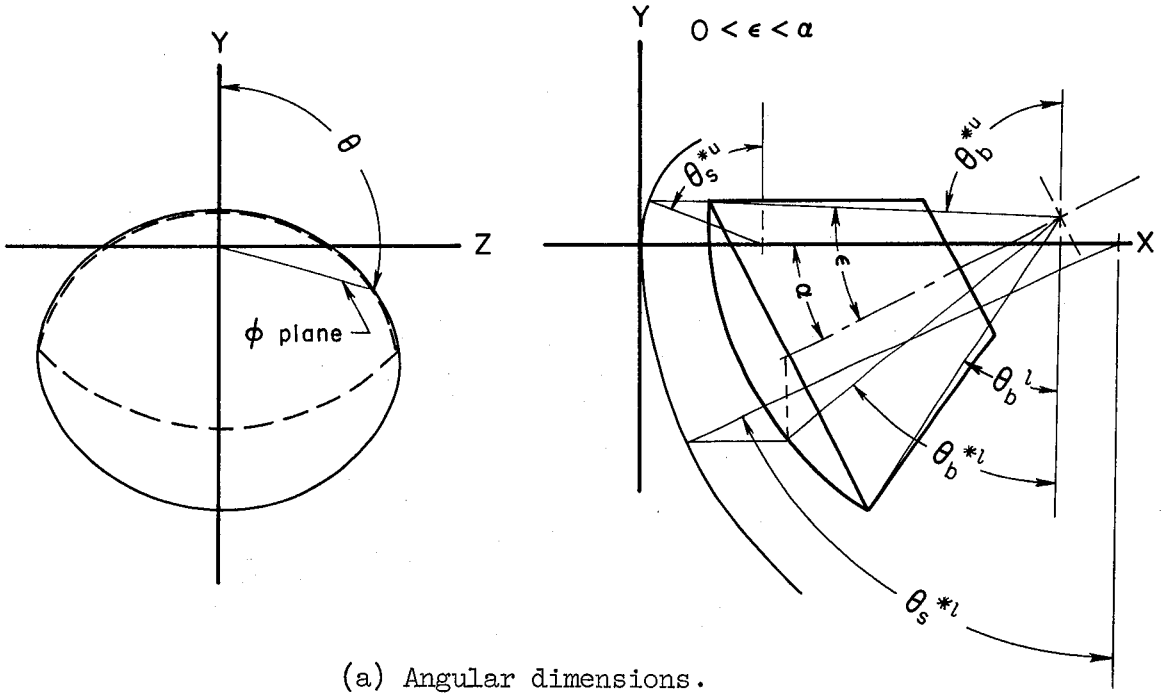

(a) Angular dimensions.

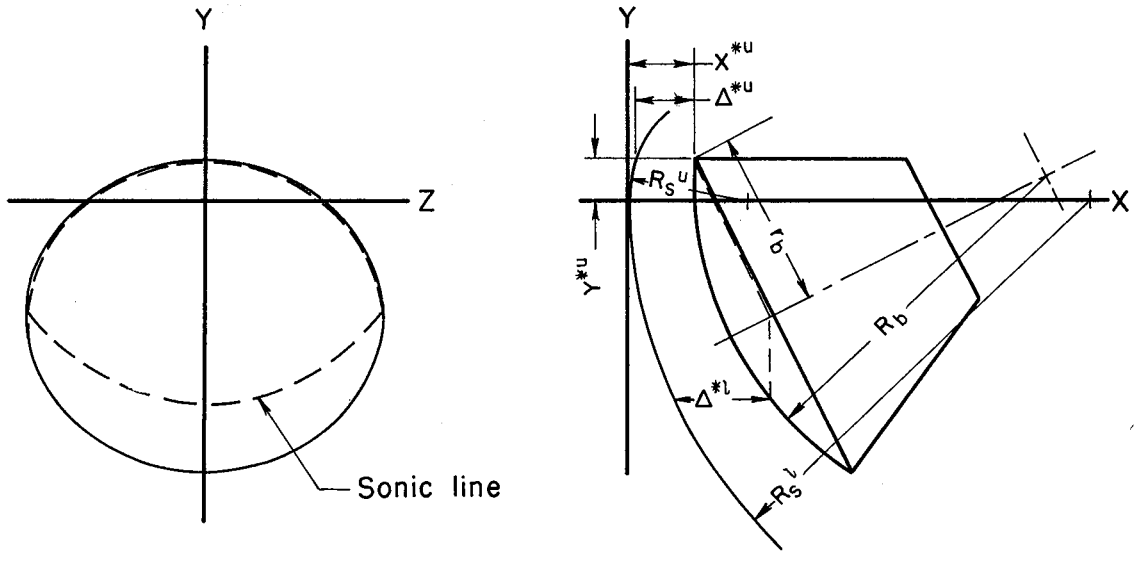

(b) Linear dimensions.

Figure 2.- Shock and vehicle geometry.

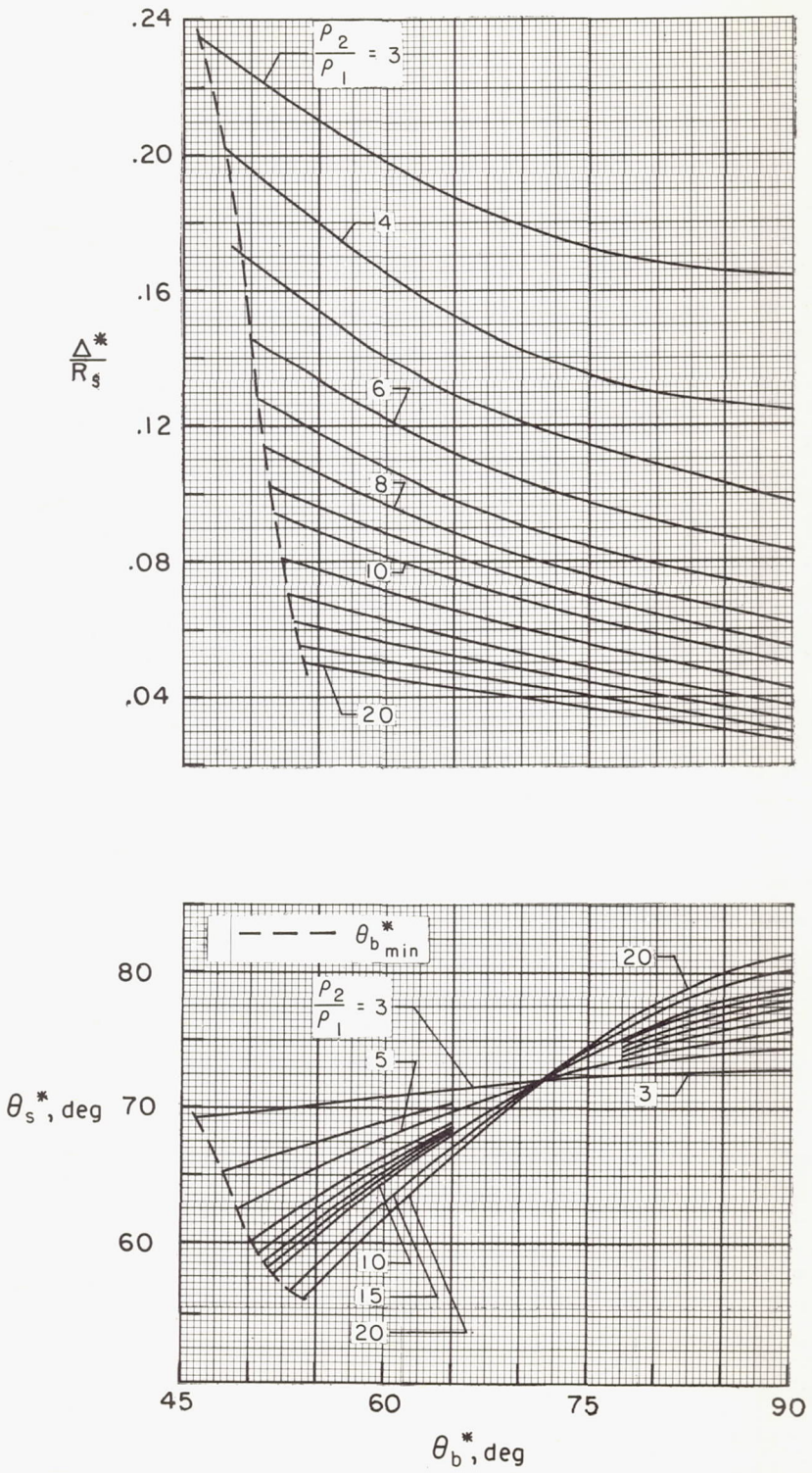

Figure 3.- Charts of shock stand-off distance and shock slope at the sonic point.

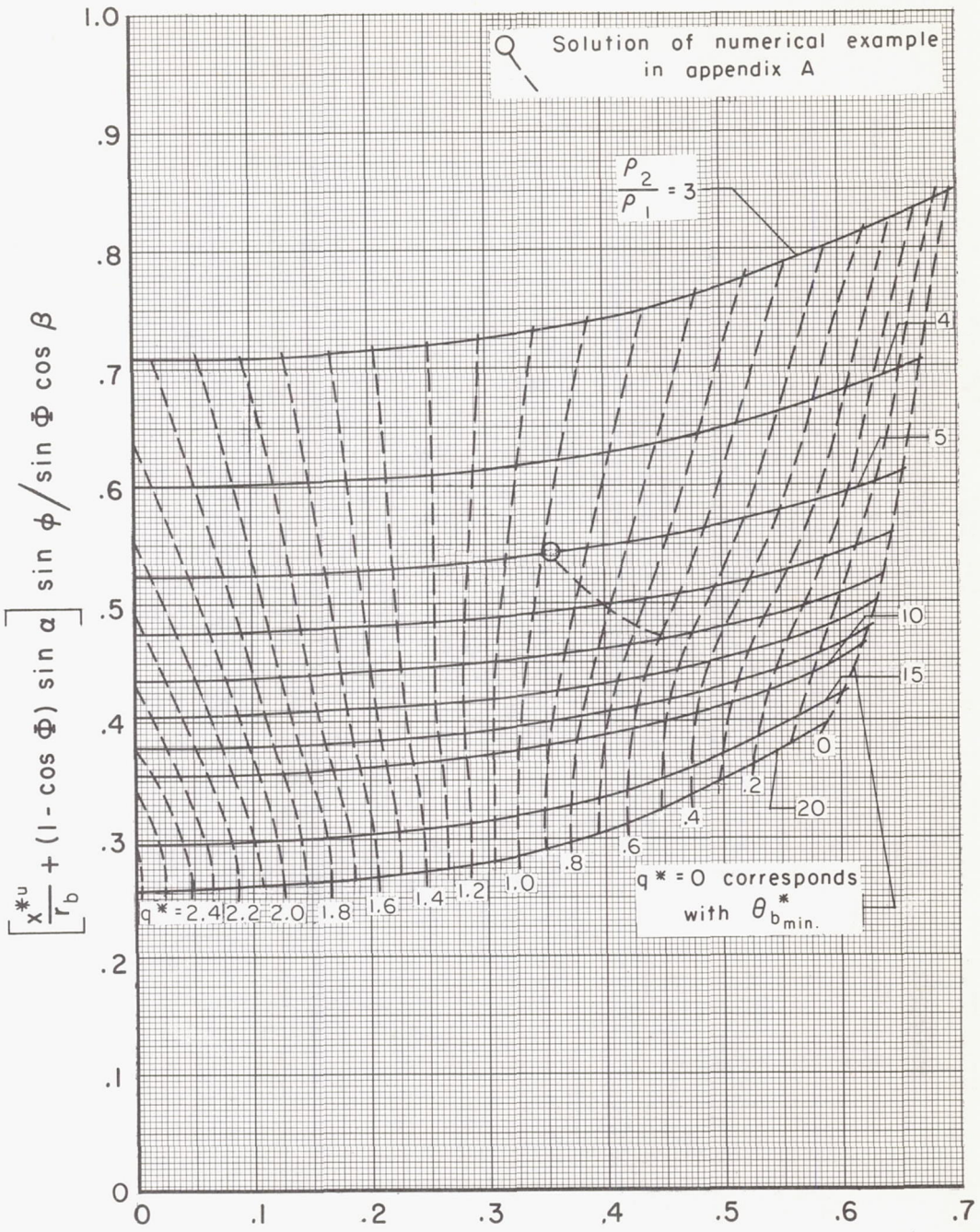

$$\cos\theta_b^* = \frac{\left\{\frac{\sin\epsilon\sin\Phi\cos\beta}{\sin\phi} - \sin\epsilon_0\cos(\phi-\beta)\right\}}{\cos\left\{\sin^{-1}\left[\frac{\sin\epsilon\sin\Phi\sin\beta}{\sin\phi} + \sin\epsilon_0\sin(\phi-\beta)\right]\right\}}$$

Figure 4.- Chart for shock solution in φ plane.

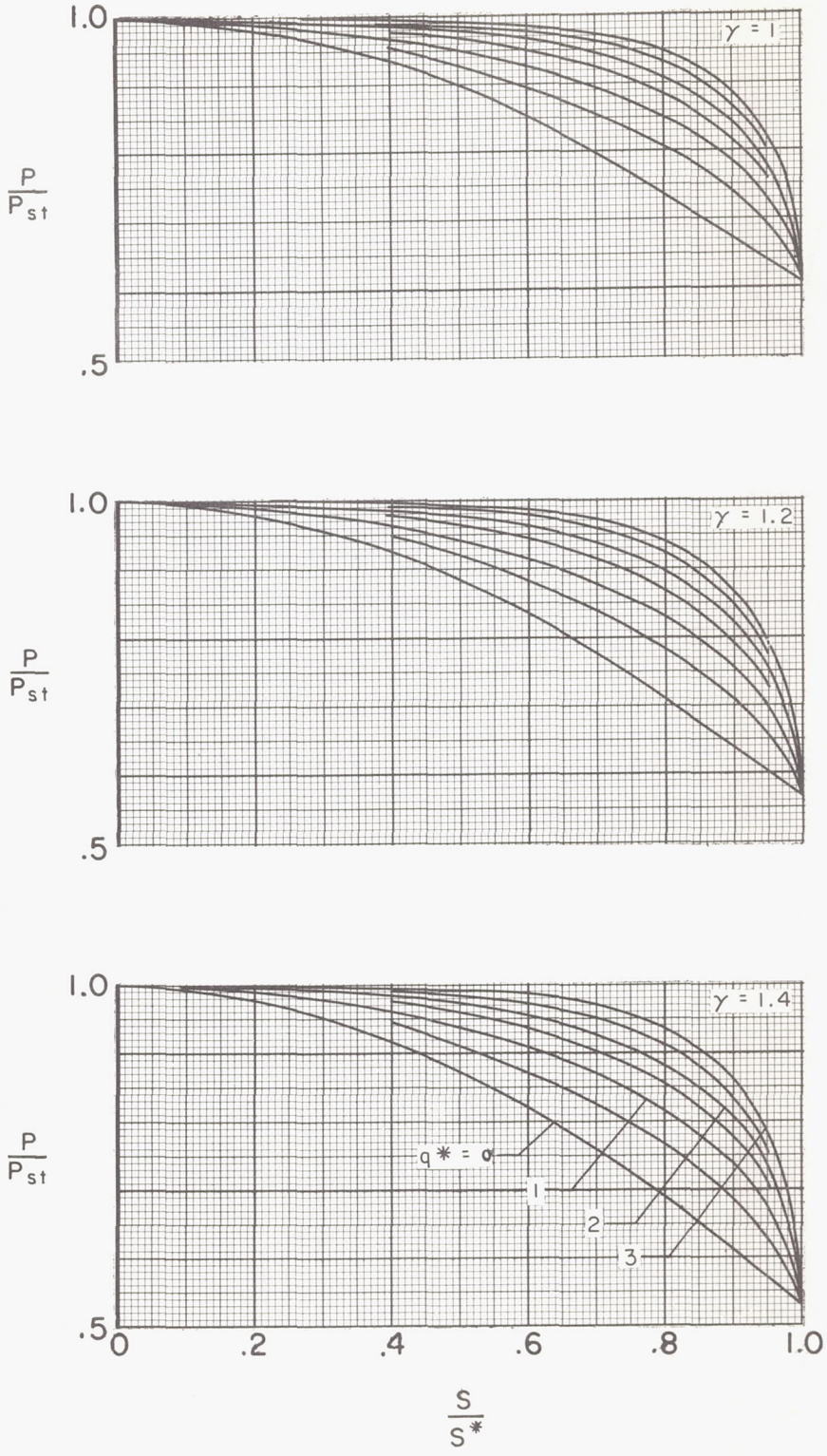

Figure 5.- Pressure distribution charts.

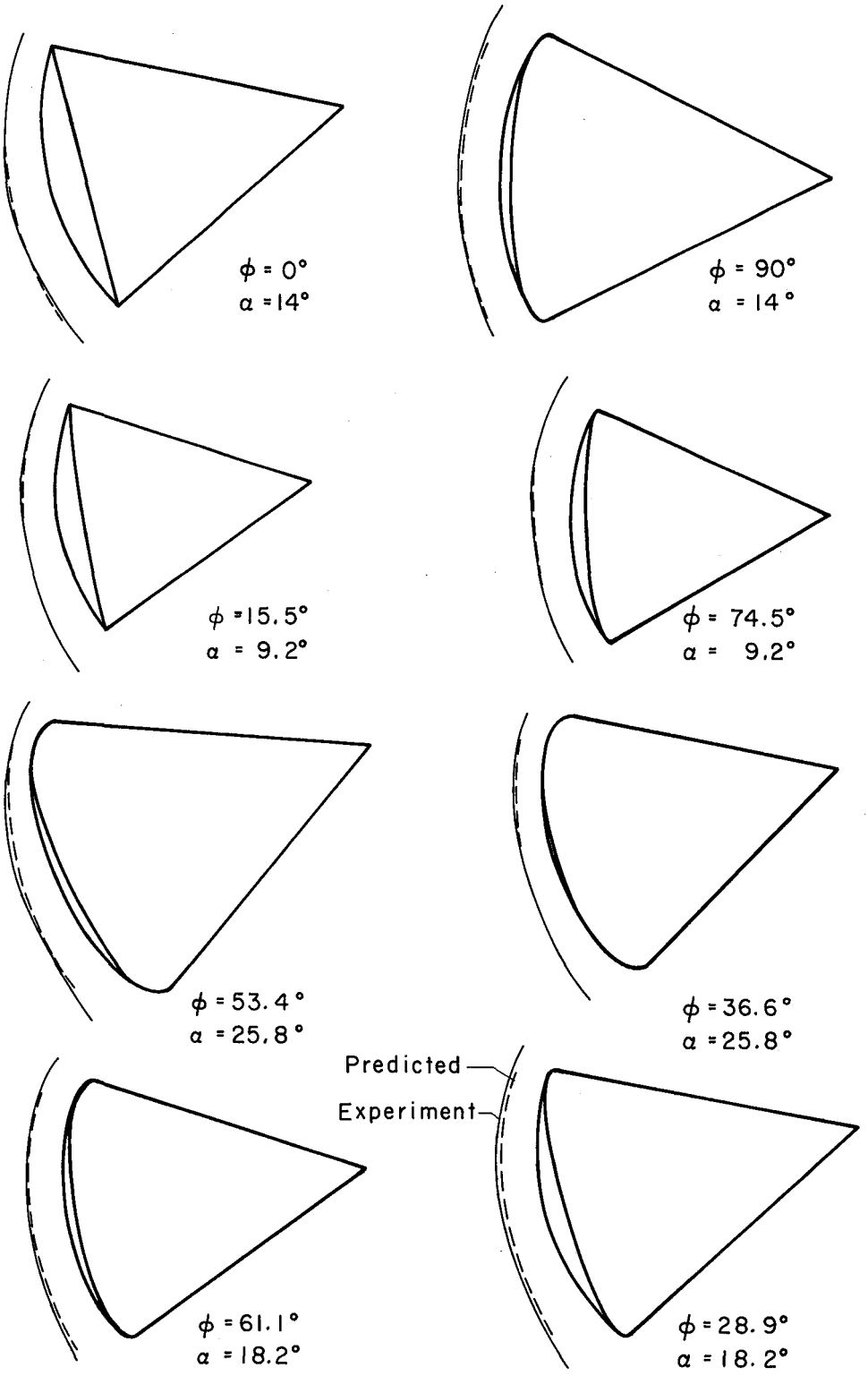

Figure 6.- Shock traces in various φ planes; $\frac{\rho_2}{\rho_1} = 5.15$, $\epsilon = 30^{\circ}$.

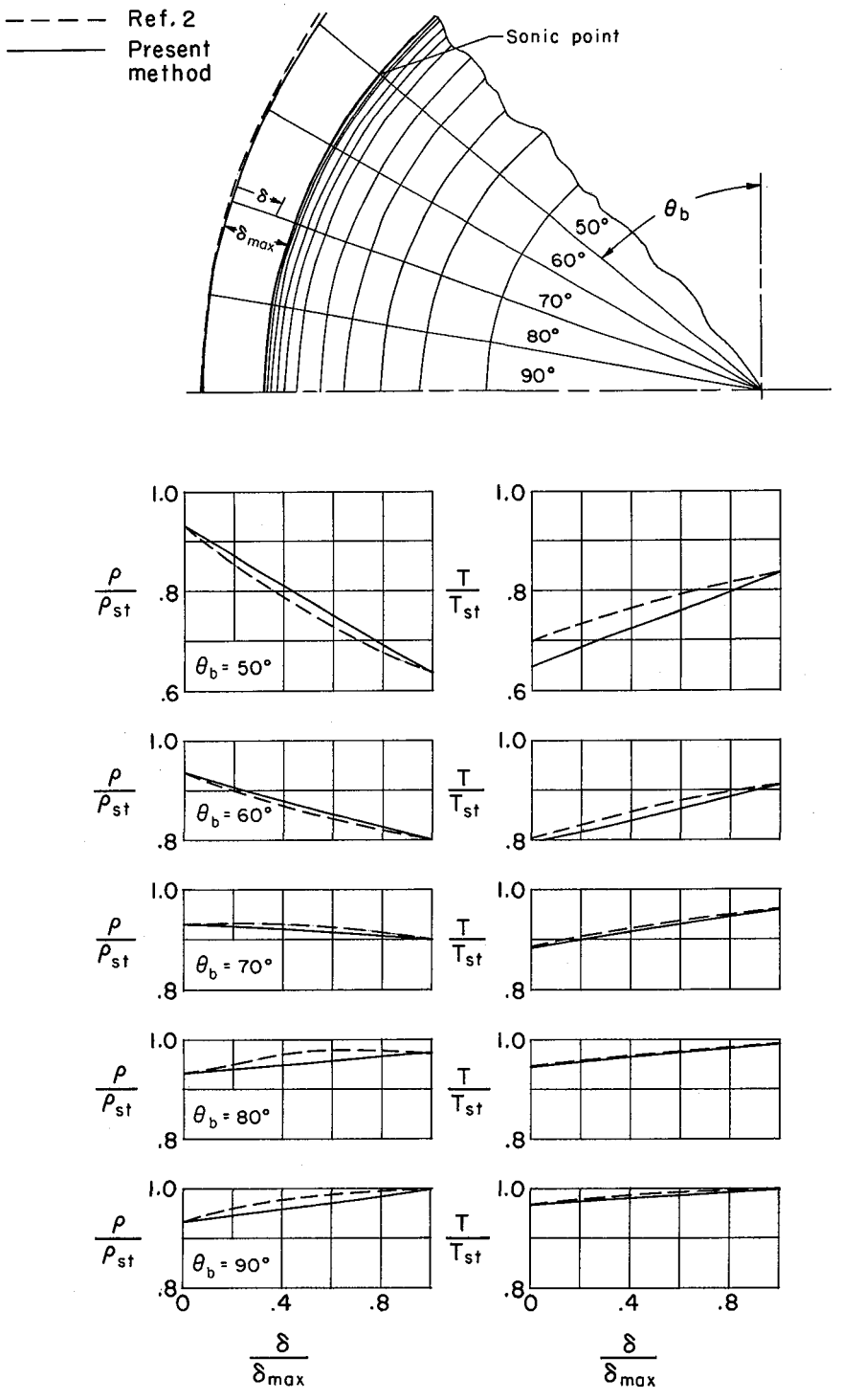

(a) $\frac{\rho_2}{\rho_1} = 6$, $\gamma = 1.4$

Figure 7.- Density and temperature in shock layer of sphere.

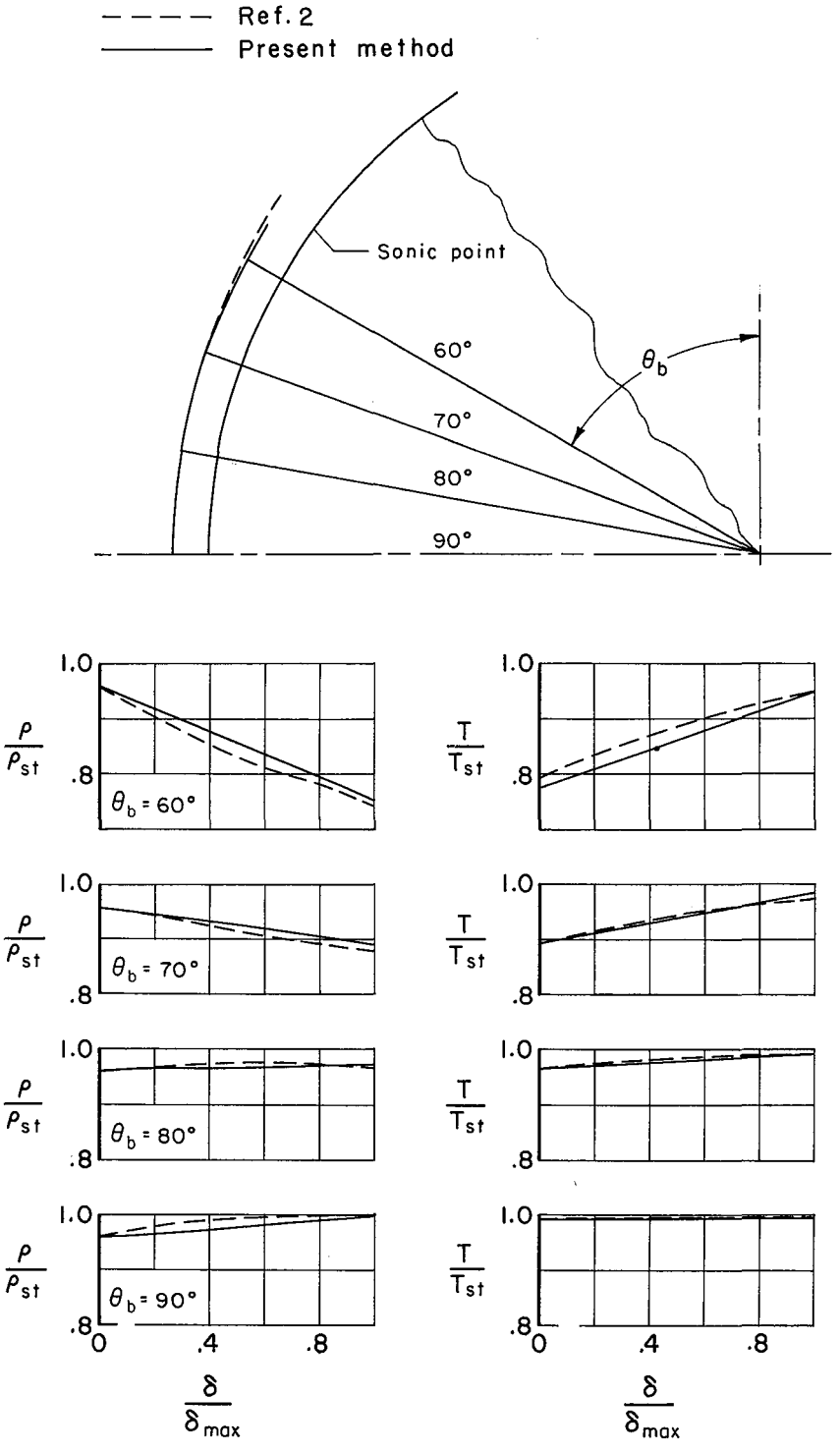

(b) $\frac{\rho_2}{\rho_1} = 11$, $\gamma = 1.2$

Figure 7.- Concluded.

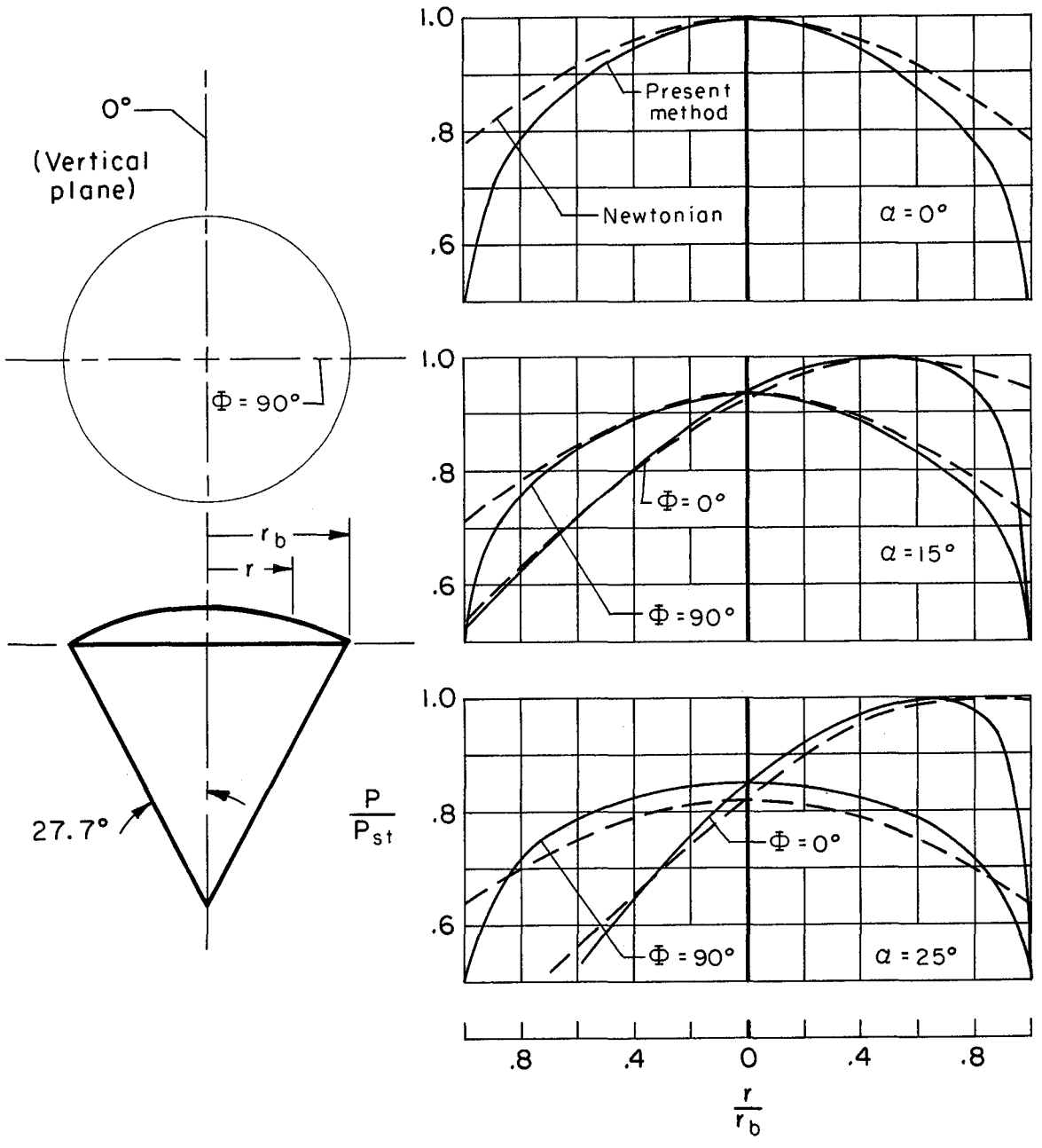

Figure 8.- Estimated pressure distributions on a capsule, M = 6 in air.

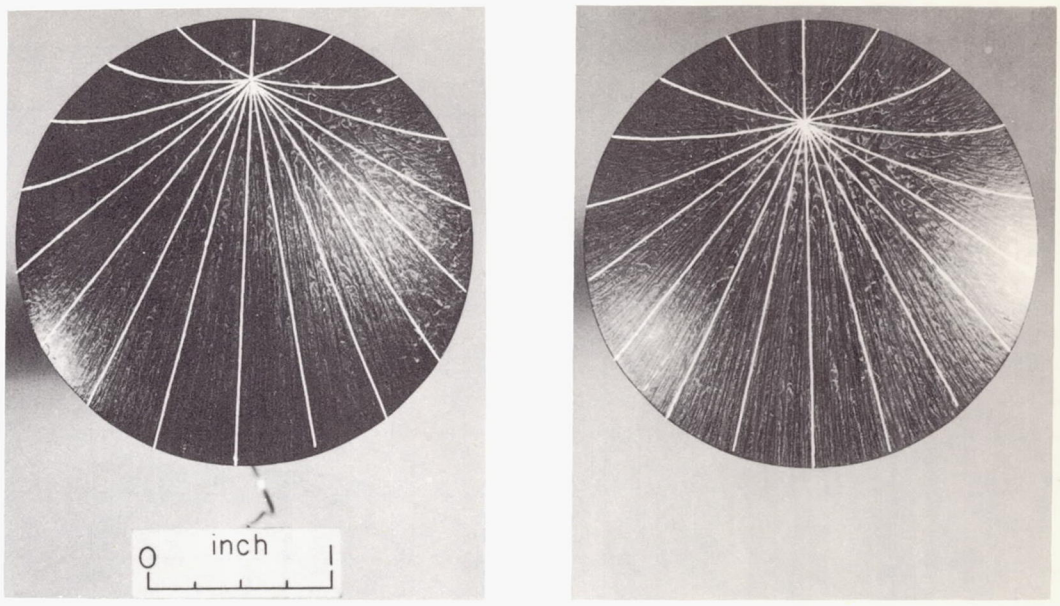

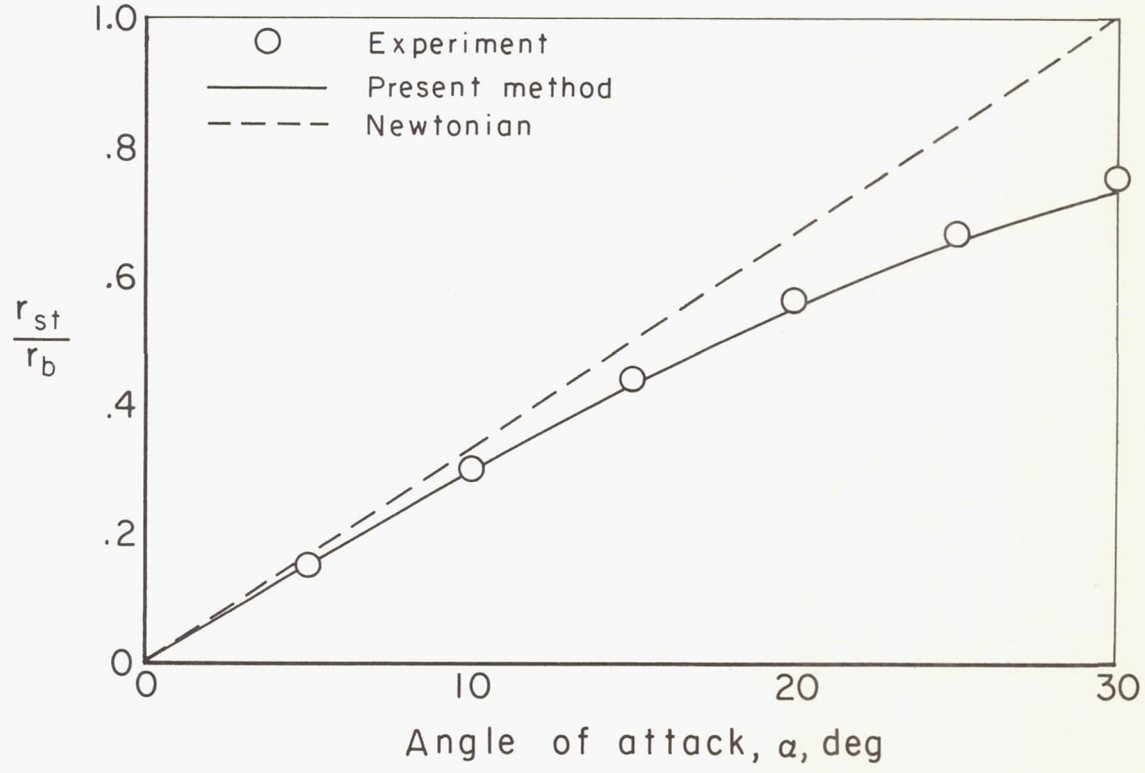

Figure 9.- Experimental and predicted stream patterns and stagnation-point locations, M = 3.3 in air.

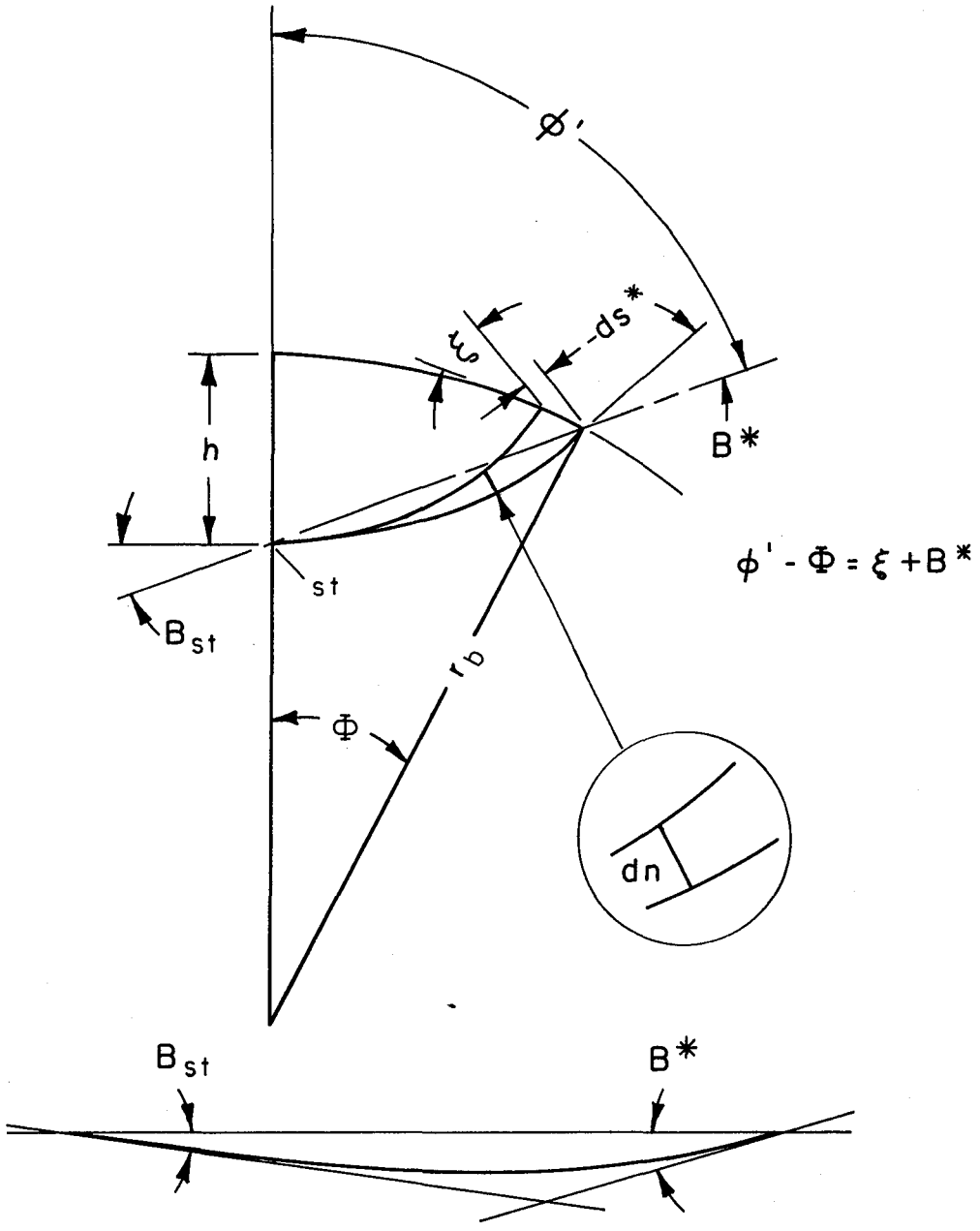

Example construction of flow curve

$B_{st} = 6°$ $B^* = 15°$

Figure 10.- Stream geometry on capsule face.

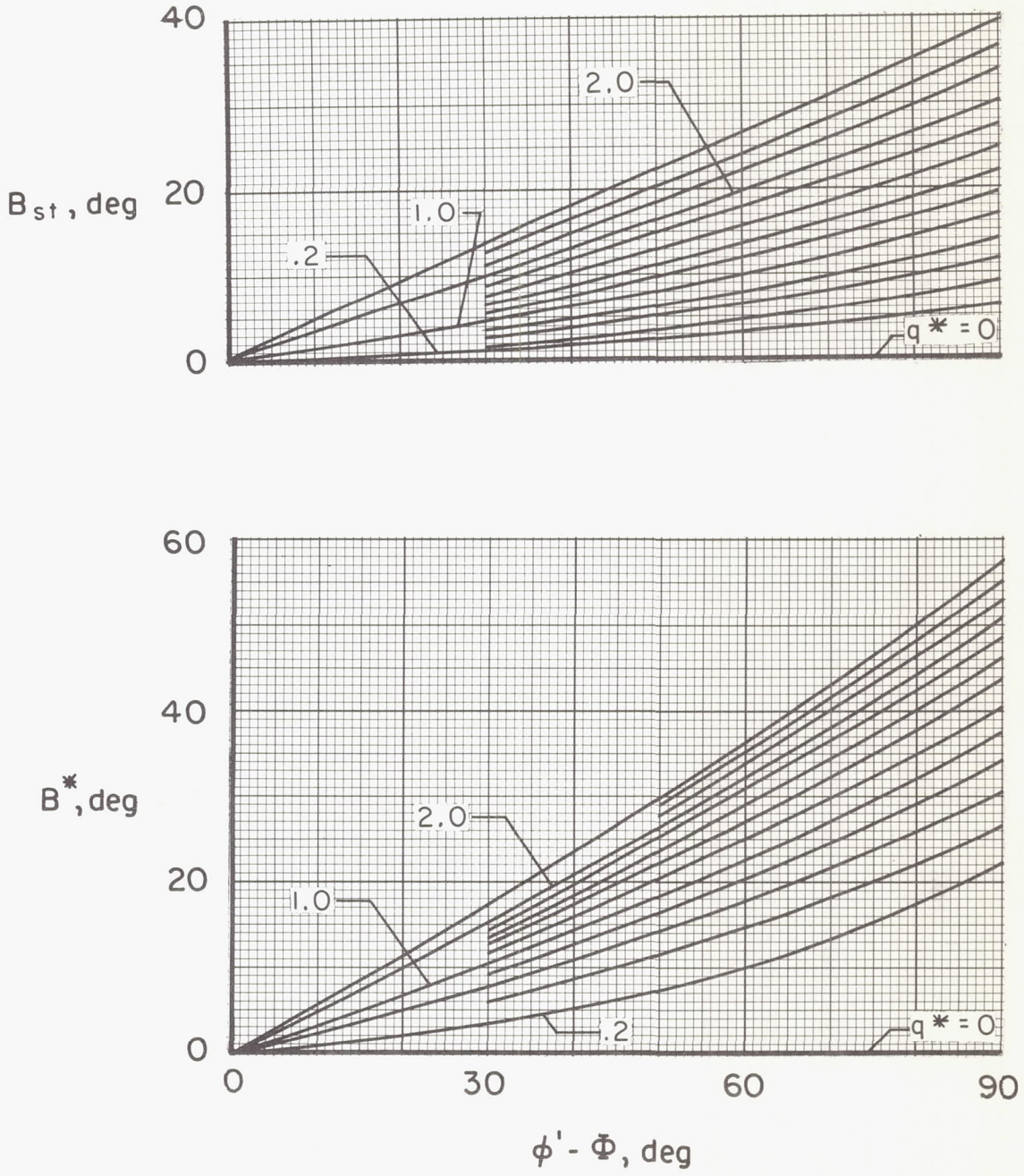

Figure 11.- Stream angles B* and B_{st} on capsule.